Available online at www.sciencedirect.com
ScienceDirect
Journal of Power Sources 161 (2006) 1030–1040
JOURNAL OF POWER SOURCES
www.elsevier.com/locate/jpowsour

Effect of inlet flow maldistribution on the thermal and electrical performance of a molten carbonate fuel cell unit

Syu-Fang Liu [a,b], Hsin-Sen Chu [a,*], Ping Yuan [b]

[a] *Department of Mechanical Engineering, National Chiao Tung University, 1001 Ta Hsueh Road, Hsinchu, Taiwan 300, ROC*
[b] *Department of Mechanical Engineering, Lee Ming Institute of Technology, 2-2 Lee Zhuan Road, Taishan, Taipei, Taiwan 243, ROC*

Received 14 April 2006; received in revised form 16 May 2006; accepted 16 May 2006
Available online 3 July 2006

Abstract

This study investigates the temperature and current density distributions in a molten carbonate fuel cell unit when the inlet flows of the anode gas and the cathode gas are mal-distributed in eight patterns. The two-dimensional simultaneous partial differential equations of mass, energy and electrochemistry are solved numerically. The results indicate that the maldistribution of anode and cathode gases dominates the current density field and the cell temperature field, respectively. Moreover, the non-uniform inlet flow slightly affects the mean temperature and mean current density, but worsens the distribution of temperature and current density for most maldistribution patterns. According to the results, the variations of the cell temperature in Pattern G and the current density in Pattern D are 12% and 37% greater than those in the uniform pattern when the deviation of the non-uniform profile is 0.25. Consequently, the effect of non-uniform inlet flow on the temperature and current density distribution on the cell plane is evident, and cannot be neglected.

Keywords: Maldistribution; Inlet flow; Molten carbonate Fuel cell; Temperature; Current density

1. Introduction

The technology of the molten carbonate fuel cell (MCFC) has received much attention in the last 2 decades, and is now at the stage of being scaled-up for commercialization. Since the MCFC operates at a high temperature of around 650 °C, the prediction of the temperature distribution is important to avoid hot spots in cells. Hot spots of extra high temperature cause electrolytic loss by corrosion and reduce the lifetime of the fuel cells. Moreover, the variation of the temperature influences the local current density, and changes the electrical performance of the MCFC. Therefore, many researchers have investigated the thermal and electrical performance of molten carbonated fuel cells.

Kobayashi et al. [1] used a numerical method to solve the steady-state temperature distribution of fuel cells with reaction areas of 900 and 3600 cm^2. They compared experimental data with numerical results, and found reasonable agreement. Yoshiba et al. [2] developed a three-dimensional numerical analysis model of cell voltage, temperature, and current profile in molten carbonate fuel cell stacks. They compared co-flow, counter-flow, and cross-flow, and found that the net output power was highest in co-flow geometry. Later, Yoshiba et al. [3] investigated the temperature and performance of molten carbonate fuel cell stacks with co-flow configuration by applying a numerical model. Their results indicated that the increase in the partial internal resistance and an insufficiency of supplied fuel gas to the cell could induce differences in cell voltage. Koh et al. [4] used a software package to predict the dynamic pressure and temperature distribution of gas in a co-flow molten carbonate fuel cell stack based on an assumption of uniform current density. The results indicated that the predicted axial velocity profile precisely reflected the mass change in MCFC, by showing a drop in the volumetric flow in the cathode and an increase in the anode. Later, Koh et al. [5] used computational fluid dynamics code to predict the temperature distribution of a co-flow MCFC stack considering the effects of radiation and variable gas properties. The results showed that the thermal radiation only weakly affects the calculation of the temperature field using the model, and most of the gas properties can be treated constant, except

* Corresponding author. Tel.: +886 3 5712121x55115; fax: +886 3 5727930.
E-mail address: hschu@cc.nctu.edu.tw (H.-S. Chu).

0378-7753/$ – see front matter © 2006 Elsevier B.V. All rights reserved.
doi:10.1016/j.jpowsour.2006.05.031

Nomenclature

a	area of heat transfer area per base area ($m^2\ m^{-2}$)
c_p	specific heat capacity ($J\ mol^{-1}\ K^{-1}$)
d	deviation of inlet flow profile, as shown in Fig. 2
E	Nernst voltage (V)
E_0	reversible open circuit voltage (V)
F	Faraday's constant (96485 $As\ mol^{-1}$)
h	heat transfer coefficient ($W\ m^{-2}\ K^{-1}$)
i	current density ($A\ m^{-2}$)
i_0	exchange current density ($A\ m^{-2}$)
$\bar{i}$	average current density in the x–y plane ($A\ m^{-2}$)
Δi	current density variation in the x–y plane ($A\ m^{-2}$)
k	conductivity ($W\ m^{-1}\ K^{-1}$)
L	length in the x or y direction, indicated by subscript x or y (m)
n	molar flow rate of anode gas or cathode gas per unit width, indicated by subscript ag or cg ($mol\ m^{-1}\ s^{-1}$)
N	molar flow rate of anode gas or cathode gas, indicated by a subscript ag or cg ($mol\ s^{-1}$)
n_e	number of electrons transferred in reactions of anode and cathode
P	pressure (Pa)
q	heat generation due to chemical reaction ($W\ m^{-2}$)
R	universal gas constant ($8.314\ J\ mol^{-1}\ K^{-1}$)
R_{tot}	total cell resistance ($\Omega\ m^2$)
T	temperature (K)
$\bar{T}$	average temperature in the x–y plane (K)
ΔT	temperature variation in the x–y plane (K)
V	cell voltage (V)
x	x direction
X	molar fraction indicated by subscript k
y	y direction

Greek symbols

δ	thickness (m)
ν	stoichiometric coefficient of k-component indicated by subscript k

Subscripts

ag	anode gas
ag-c	interface between anode gas and cell
ag-s	interface between anode gas and separator
c	cell
c–s	interface between cell and separator
eg	cathode gas
cg-c	interface between cathode gas and cell
cg-s	interface between cathode gas and separator
k	components in anode gas or cathode gas
s	separator
x	x direction
y	y direction

for the specific heat capacity of the anode gas. He and Chen [6] investigated the three-dimensional temperature distribution, the pressure, the gas concentration, and the current density of a molten carbonate fuel cell of five stacks with three manifolds, using CFD software. The results indicated that the temperature was maximum at different locations under co-flow, counter-flow, and cross-flow configurations. The maximum temperature difference between among the flow configurations is 10–20 °C. Subsequently, He and Chen [7] extended their simulation to investigate the transient behavior of an MCFC stack with the cross-flow configuration; the results showed that the current density profile changes rapidly in the beginning and slowly in the following stage, and the temperature response is slow when the MCFC was under a step voltage change.

For over-potential from the anode gas to the cathode gas, Bosio et al. [8] presented a model and experimental investigation of electrochemical reactors in the molten carbonate fuel cell. Additionally, they used their formula for total cell resistance, tested with experimental data, to analyze the temperature distribution and current density distribution for a single cell and stacks, using Fortran program. Their numerical results agree with the experimental results, and showed that the thermodynamics fails to predict the open circuit voltage because of the effects of gas crossover phenomena at the cell level. Although thermodynamic equilibrium should be established under open circuit conditions in principle, short circuit electrical currents circulate within the cell, and the consequent voltage loss is responsible for irreversibility. Arato et al. [9] investigated the limitation on the performance of molten carbonate fuel cells due to gas diffusion phenomena in the porous electrodes when high reactant utilization factors are used. The expression of voltage decay depends on concentration polarization due to hydrogen and carbon dioxide, while oxygen diffusion effects have been considered to be negligible. Furthermore, the limiting diffusion conditions must also be correctly evaluated for the local temperature and pressure drops. Recently, Mangold and Sheng [10] applied a reduced nonlinear model to solve a planar molten carbonate fuel cell with cross-flow. Since the reduced model was of the lower order than the original model, it markedly reduced the computational time. Therefore, this model was suitable for application in predicting the behavior of a control system. Lee et al. [11] calculated the temperature distribution, hydrogen conversion, and current density distribution of a unit molten carbonate fuel cell using constant voltage and constant current density methods. The results indicated that cell performance calculated by the constant voltage method fit better the experimental data than that calculated by the constant current density method.

Bosio et al. [12] reported the development of molten carbonate fuel cell technology at Ansaldo Ricerche, from small-scale single cell up to stacks of several KW capacities, for industrial applications. Although the report showed that MCFC technology had been successfully tested on stacks in the kW power class, the control of the start-up phase, electrolyte migration through the manifolds and gas feed distribution have not yet been to be solved. Notably, the gas feed distribution in [12] identified the variation of mole flow rate in different stacks. Hence, the stack nearest the anode gas inlet duct has largest flow rate and the far-

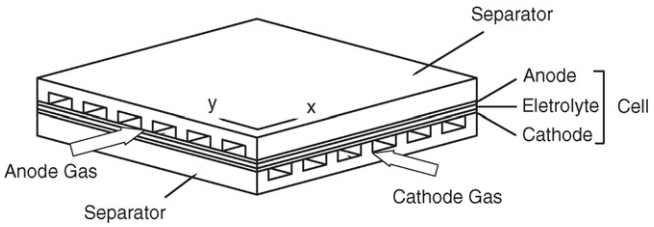

Fig. 1. Schematic diagram of a molten carbonate fuel cell unit in crossflow.

thest one has the lowest. The cross-sectional geometry of a fuel cell is similar to that of a heat exchanger, whose inlet distributor is responsible for a non-uniform flow distribution in the frontal area. Therefore, the maldistribution of the inlet flow rate on the frontal area is realistic and it must affect the performance of fuel cells. Hirata and Hori [13] adopted a numerical method to examine the relationships among the gas flow uniformities in the planar direction, the gas flow uniformity in the stacking direction, and the cell performance in a co-flow MCFC. Although their results showed that the gas flow uniformity in the stacking direction is about 2–10 times that in the planar direction, we believe that the maldistribution of inlet flow in the planar direction will produce a more complex temperature distribution and current density distribution because of the cross-flow pattern. Therefore, this study investigates the temperature and current density fields of a unit MCFC with different non-uniform inlet flow patterns in the crossflow configuration.

2. Analysis

2.1. Physical model

This study investigates a unit of a molten carbonate fuel cell with an area of 0.6 m × 0.6 m when the anode gas and the cathode gas flow in the cross-flow configuration, in which the anode gas flows in the x direction, and the cathode gas flows in the y direction, as shown in Fig. 1. The ribs of separator cause the anode gas and the cathode gas to flow without mixing: each flow is considered to composed of many flow tubes that are parallel to each other. As mentioned above, the position of the manifold may induce different maldistributions of the flow rate in the inlet cross-section. This study considers a uniform profile, a progressively decreasing profile, and a progressively increasing profile to construct eight patterns of non-uniform inlet flow, as shown in Fig. 2. The term d represents the unilateral deviation of the non-uniform profile, which is the ratio of the variation of flow rate in one side to the mean flow rate. The formulations of the governing equations are based on the following assumptions. (1) The inlet temperature and molar fractions of species in the anode gas and the cathode gas are constant and uniform. (2) The thermal properties of the anode gas, the cathode gas, the cell and the separator are constant, except for the specific heat capacities of the anode gas and the cathode gas. (3) The boundaries of the cell and separator are adiabatic. (4) The change in the z direction is negligible. (5) The cross-sectional geometry of separator is unchanged throughout the x–y plane. (6) The water-shift reaction in the anode gas is negligible. (7) The cell voltage is uniform over the cell plane.

2.2. Governing equations

2.2.1. Reaction equations

This study considers a molten carbonate fuel cell unit with external reforming: the reforming reaction in the anode gas is neglected. The cathode gas is the air obtained from the atmosphere, and the electricity is generated in the cell, which includes the anode, the electrolyte and the cathode. Meanwhile, the electrolyte is a porous matrix that contains migrating ions of molten carbonate. The reactions in the anode and the cathode are as follows.

$$H_2 + {CO_3}^{2-} \rightarrow HO_2 + CO_2 + 2e^- \quad (1)$$

$$O_2 + 2CO_2 + 4e^- \rightarrow 2{CO_3}^{2-} \quad (2)$$

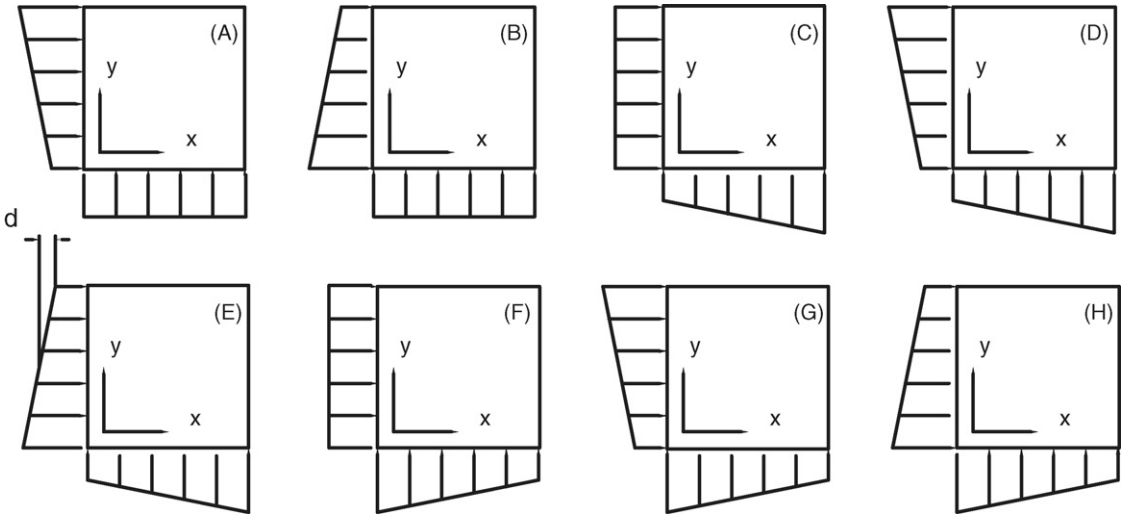

Fig. 2. Patterns of non-uniform inlet flow profile in this study.

2.2.2. Mass conservation equations

The relationship between the current density and gas molar flux for species at the electrodes surface is described from Faraday's law. Therefore, the mass balances of the anode and the cathode gases are as follows:

$$\frac{1}{L_y}\frac{\mathrm{d}n_{\mathrm{ag},k}}{\mathrm{d}x} = \pm\frac{i}{n_\mathrm{e}F} \tag{3}$$

$$\frac{1}{L_x}\frac{\mathrm{d}n_{\mathrm{cg},k}}{\mathrm{d}y} = \pm\frac{i}{n_\mathrm{e}F} \tag{4}$$

where n is the mole flow rate of the k-component, and n_e is the number of electrons transferred in the reactions of the anode and the cathode. The plus/minus symbol represents an increase/decrease in each species' mole flow rate caused by the chemical reaction in the anode and the cathode. It is positive for reactants, and negative for products in the anode and the cathode.

2.2.3. Energy conservation equations

This work applies the conservation of energy for anode gas, cathode gas, the cell and the separator. For anode gas,

$$\frac{\mathrm{d}}{\mathrm{d}x}\left(\sum n_{\mathrm{ag},k}c_{\mathrm{p},k}T_\mathrm{ag}\right) = \dot{q}_{\mathrm{conv,s-ag}} + \dot{q}_{\mathrm{conv,c-ag}} + \dot{q}_{\mathrm{mass,c-ag}} \tag{5}$$

For cathode gas,

$$\frac{\mathrm{d}}{\mathrm{d}y}\left(\sum n_{\mathrm{cg},k}c_{\mathrm{p},k}T_\mathrm{cg}\right) = \dot{q}_{\mathrm{conv,s-cg}} + \dot{q}_{\mathrm{conv,c-cg}} - \dot{q}_{\mathrm{mass,cg-c}} \tag{6}$$

For the cell,

$$(k\delta)_\mathrm{c}\frac{\partial^2 T_\mathrm{c}}{\partial x^2} + (k\delta)_\mathrm{c}\frac{\partial^2 T_\mathrm{c}}{\partial y^2} - \dot{q}_\mathrm{cont} - \dot{q}_{\mathrm{conv,c-ag}} - \dot{q}_{\mathrm{conv,c-cg}} + \dot{q}_{\mathrm{mass,cg-c}} - \dot{q}_{\mathrm{mass,c-ag}} + \dot{q}_\mathrm{reac} = 0 \tag{7}$$

For the separator,

$$(k\delta)_\mathrm{s}\frac{\partial^2 T_\mathrm{s}}{\partial x^2} + (k\delta)_\mathrm{s}\frac{\partial^2 T_\mathrm{s}}{\partial y^2} + \dot{q}_\mathrm{cont} - \dot{q}_{\mathrm{conv,s-ag}} - \dot{q}_{\mathrm{conv,s-cg}} = 0 \tag{8}$$

where the heat transfer rate terms are described in Table 1. In Eqs. (3)–(6), this study considers the molar flow rate of the anode gas and cathode gas are a progressively decreasing profile, a progressively increasing profile, or a uniform profile in the inlet. The inlet conditions are described as follow.

$$n_\mathrm{ag}(0, y) = \frac{N_\mathrm{ag}}{L_y}\left(\frac{2d}{L_y}y + 1 - d\right) \tag{9}$$

$$n_\mathrm{cg}(x, 0) = \frac{N_\mathrm{cg}}{L_x}\left(\frac{2d}{L_x}x + 1 - d\right) \tag{10}$$

where N_ag and N_cg are the total molar flow rate of the anode gas and the cathode gas, respectively, from inlet ducts, and the deviation of d may be negative, zero, and positive, which represents the progressively decreasing profile, uniform profile, and progressively increasing profile, respectively. In Table 1, $k_{\mathrm{c-s}}$ is the thermal conductivity due to the contact resistance between the cell and the separator in the z direction. The thermal conductivity, $k_{\mathrm{c-s}}$, is set to 1.0 W m^{-1} K^{-1} [1].

2.2.4. Nernst voltage and polarizations

The Nernst voltage is calculated using the Nernst equation, as follows:

$$E = E_0 + \frac{RT}{2F}\ln\left(\frac{P_{\mathrm{H_2}}P_{\mathrm{O_2}}^{0.5}P_{\mathrm{CO_2,cg}}}{P_{\mathrm{H_2O}}P_{\mathrm{CO_2,ag}}}\right) \tag{11}$$

$$E_0 = 1.2723 - 2.7654\times10^{-4}T \tag{12}$$

Meanwhile, E_0 is the reversible voltage under standard conditions. According to the results in [8], this study uses the total cell resistance, including that due to cathode polarization, the electrolyte tile contribution, and the Ohmic resistance of the contacts. Note that this total cell resistance did not include the concentration polarization, because [8] assumed the diffusion is non-limiting in the electrode. The cell voltage is the Nernst voltage minus the over-potentials, as follows:

$$V = E - iR_\mathrm{tot} \tag{13}$$

$$R_\mathrm{tot} = \frac{A\mathrm{e}^{B/T}}{\Pi_\mathrm{i}p_\mathrm{i}^{\beta_\mathrm{i}}} + c_\mathrm{ir} + D\,\mathrm{e}^{F/T} \tag{14}$$

where the parameters are $\beta^{\mathrm{O_2}} = 0.67$, $A = 1.38\times10^{-7}$ Ωm^2 Pa$^{0.67}$, $B = 11400$ K, $c_\mathrm{ir} = 0.348\times10^{-4}$ Ωm^2, $D = 4.8\times10^{-8}$ Ωm^2 and $F = 6596$ K [8].

Table 1
Expressions of energy source terms in energy conservation Eqs. (5)–(8)

Symbols	Description	Expression
$\dot{q}_{\mathrm{conv,s-ag}}$	Heat transfer rate from separator to anode gas by convection	$(ha)_{\mathrm{s-ag}}(T_\mathrm{s} - T_\mathrm{ag})$
$\dot{q}_{\mathrm{conv,s-cg}}$	Heat transfer rate from separator to cathode gas by convection	$(ha)_{\mathrm{s-cg}}(T_\mathrm{s} - T_\mathrm{cg})$
$\dot{q}_{\mathrm{conv,c-ag}}$	Heat transfer rate from cell to anode gas by convection	$(ha)_{\mathrm{c-ag}}(T_\mathrm{c} - T_\mathrm{ag})$
$\dot{q}_{\mathrm{conv,c-cg}}$	Heat transfer rate from cell to cathode gas by convection	$(ha)_{\mathrm{c-cg}}(T_\mathrm{c} - T_\mathrm{cg})$
$\dot{q}_{\mathrm{mass,c-ag}}$	Heat transfer rate due to ion migration from cell to anode gas	$\frac{i}{2F}c_{p,\mathrm{CO_3^{2-}}}T_\mathrm{c}$
$\dot{q}_{\mathrm{mass,cg-c}}$	Heat transfer rate due to ion migration from cathode gas to cell	$\frac{i}{2F}c_{p,\mathrm{CO_3^{2-}}}T_\mathrm{cg}$
$\dot{q}_\mathrm{cont}$	Heat transfer rate from cell to separator by contact conduction	$(ka)_{\mathrm{c-s}}\frac{(T_\mathrm{c}-T_\mathrm{s})}{\delta_{\mathrm{c-s}}}$
$\dot{q}_\mathrm{reac}$ [16]	Heat generation rate due to chemical reaction	$-\Delta H\frac{i}{2F} - Vi$ $\Delta H = -240506 - 7.3835T_\mathrm{c}$

The above simultaneous equations of the MCFC contain seven unknown variables, which are mole flow rate of each species ($n_{ag,k}$ and $n_{cg,k}$), anode gas temperature (T_{ag}), cathode gas temperature (T_{cg}), cell temperature (T_c), separator temperature (T_s), current density (i), and cell voltage (V). The mass equations are used to determine mole flow rate of each species, and energy equations are used to determine the temperatures. Nevertheless, in Eq. (13), both current density and cell voltage variables must be evaluated. Therefore, this study assumes that the cell voltage is uniform over the reaction area of the cell and then calculates the current density using Eq. (13).

3. Simulation

This study divides the calculation domain of the x–y plane into N × N subdivisions, and assigns the calculation nodes of $n_{ag,k}$ and T_{ag} at the inlet and outlet of each subdivision in the x direction of the anode gas flowing. Similarly, the calculating nodes of $n_{cg,k}$ and T_{cg} are assigned to the inlet and outlet of each subdivision in the y direction of the cathode gas flowing. Furthermore, the calculation nodes of i, T_c, and T_s are assigned to the center of the subdivision. Grid generation and the implicit scheme are adopted to discretize Eqs. (3)–(8) to finite difference equations, and then employs TDMA (Tri-Diagonal Matrix Algorithm) to solve simultaneous algebraic equations. This node arrangement avoids the need to apply the upwind method to treat the first-order differential terms, and has been used to calculate the temperature fields of a three-gas cross-flow heat exchanger [14]. The calculation proceeds as follows: (1) The program guesses a uniform current density distribution and solves the mole flow rate of each species in the anode gas and the cathode gas using Eqs. (3) and (4). (2) The program solves the temperature fields of the anode gas, the cathode gas, the cell, and the separator using Eqs. (5)–(8), respectively. (3) The Nernst voltage and internal total resistance are calculated using Eqs. (11) and (14), and then the current density is obtained from Eq. (13) by setting the cell voltage to a constant value. (4) The current density is updated to Step 1, and the loop iterated from Steps 1 to 4 until all relative errors of the mole flow rates, the temperature and the current density satisfy the converge criterion. FlexPDE software was used to solve the Eqs. (3)–(14), to verify the accuracy of calculation, because FlexPDE is a flexible solver of partial differential equations by the finite element method.

Fig. 3 depicts the temperature distribution of the cell calculated both numerically method and using FlexPDE software at a cell voltage of 0.8 V. In this numerical method, the grid dimension depends on the mole flow rates of the anode gas and the cathode gas, and must increase as the mole flow rate falls to avoid the negative values in the finite difference equations [15]. In this comparison case, the numerical program sets the grid dimensions to be 400 × 400 with a convergence criterion of 1×10^{-5}, and FlexPDE uses 1972 elements with a convergence criteria of 0.002. The continuous lines clearly match the dashed lines in this figure. Therefore, the numerical method for calculating the temperature field is reliable. In the electrical performance calculation, Fig. 4 shows the current density distributions calculated by the numerical method herein this study and using

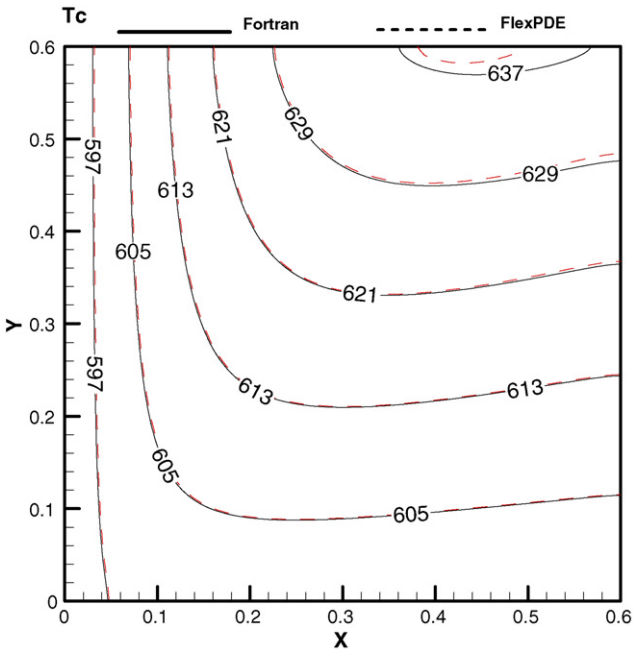

Fig. 3. Cell temperature distribution calculated by the numerical method in this study and FlexPDE software with uniform inlet flow rate.

FlexPDE software. Similarly, the continuous lines coincide with the dashed lines over the whole x–y plane. Consequently, the numerical calculation of electrical performance is also reliable. Table 2 lists all parameters and conditions in the comparison case and references relevant literature. Meanwhile, the effective contact thickness between the cell and the separator is the average thickness of the cell and the separator. Furthermore, this study uses Nu = 3.35 to estimate the convection heat transfer

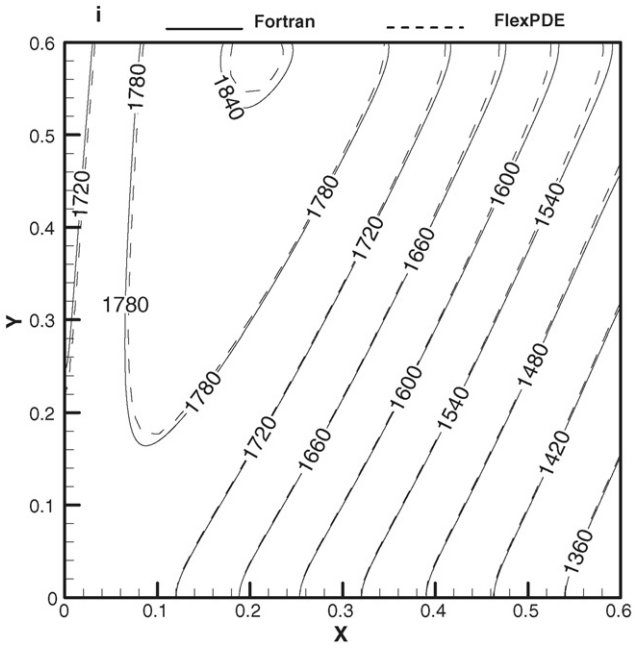

Fig. 4. Current density distribution calculated by the numerical method in this study and FlexPDE software with uniform inlet flow rate.

Table 2
Parameters and conditions in this study

Mole flow rate and molar fraction of species in anode inlet [8]	
N_{ag}	0.0621 mol/s
X_{H_2}	0.203
X_{CO_2}	0.064
X_{H_2O}	0.15
X_{N_2}	0.583
Mole flow rate and molar fraction of species in cathode inlet [8]	
N_{cg}	0.1841 mol/s
X_{O_2}	0.167
X_{N_2}	0.698
X_{CO_2}	0.135
Inlet temperature [8]	
T_{ag}	858 K
T_{cg}	867 K
Operation pressure [8]	
P	3.5×10^5 Pa
Heat transfer area per unit area [1]	
$a_{ag-s} = a_{cg-s}$	1.26 $m^2\ m^{-2}$
$a_{ag-c} = a_{cg-c}$	0.53 $m^2\ m^{-2}$
a_{c-s}	0.47 $m^2\ m^{-2}$
Conductivity [5,1]	
k_c	9 $W\ m^{-1}\ K^{-1}$
k_s	25 $W\ m^{-1}\ K^{-1}$
k_{c-s}	1.0 $W\ m^{-1}\ K^{-1}$
Thickness [11]	
δ_c	0.0023 m
δ_s	0.002 m
δ_{c-s}	0.00215 m

coefficient because the flows of anode gas and cathode gas are fully developed and laminar.

4. Results and discussion

Fig. 3 depicts the temperature distribution of the cell when the inlet flows are uniform. The isotherm increases from under 600 °C close to both the inlets of the anode gas and the cathode gas to 638 °C near the corner of both gases outlets. When the anode gas and the cathode gas flow through the reaction area of the cell, they not only supply the reaction species but also carry away the reaction heat in the cell. Therefore, the anode gas and the cathode gas accumulate all of the reaction heat and reach their maximum temperatures when they flow to the outlets. The temperatures of the gases also influence the temperature distribution of the cell and separator because coupled heat transfer occurs among them. In this figure, the isotherm in the y direction increases more uniformly than that in the x direction. Hence, the cathode gas dominates the cell cooling because it has a higher flow rate than the anode gas.

Fig. 4 displays the current density distribution on the cell plane under the same conditions as in Fig. 3. The minimum is 1316 A m^{-2} in the corner of the cathode gas inlet and the anode gas outlet, and the maximum is 1846 A m^{-2} in the middle-left outlet of the cathode gas. When the cell voltage is set to be a constant, the Nernst voltage and the internal resistance of the

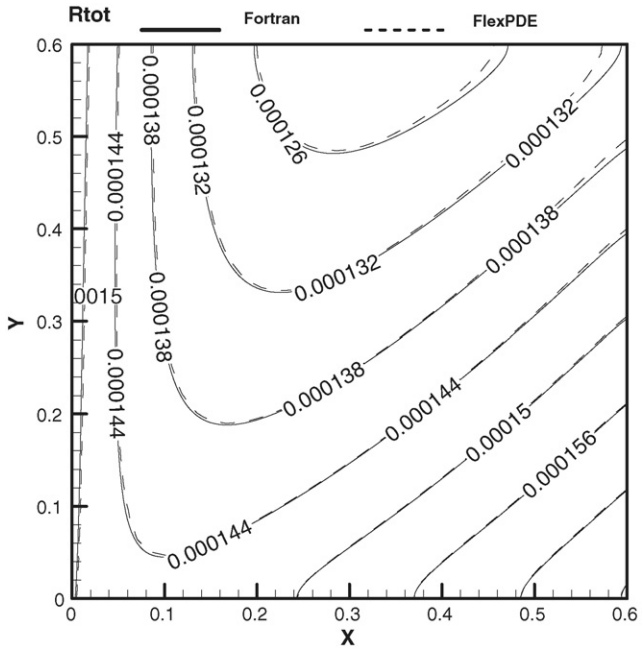

Fig. 5. Total resistance distribution on the cell plane with uniform inlet flow.

cell directly affect the current density according to the Ohmic law. With respect to the relationship between the Nernst voltage and the current density, examining the Eq. (11) indicates that the concentration of gas species influences the Nernst voltage, which declines as the concentrations of hydrogen and oxygen drop. Since the cathode gas is easily obtained from the environment and thus has a larger flow rate in order to cool the cell, the change of the concentration of oxygen is less than that of hydrogen. Consequently, the current density fell should decrease in the x direction of the anode gas flow, because the Nernst voltage fell with the drop in hydrogen concentration. With respect to the relationship between internal resistance and current density, Fig. 5 presents the total internal resistance distribution on the cell plane calculated using Eq. (14) obtained from the study of [8]. In this figure, the continuous and dashed lines match well with each other, which represents the results of Fortran program and FlexPDE, respectively. In Fig. 5, it shows that the distribution of resistance is similar to the distribution of current density, but reaches a minimum in the middle-right outlet of cathode gas. The area of lower internal resistance represents it has higher current density when the cell voltage is set to be constant. When both the effect of the concentration of species and the total internal cell resistance are considered, it is reasonable that the contour with maximum current density moves left as determined by comparing Fig. 5 to Fig. 4 because of the effect of the concentration of hydrogen.

Fig. 6(a–h) show the systematic cell temperature distribution of eight patterns with a deviation of 0.5. Meanwhile, $\bar{T}$ and ΔT represent the average and variation of cell temperature, respectively. In these figures, it shows that the dominated factor on cell temperature distribution is the cathode gas, because the main trend of isotherm is increasing along the y direction of cathode gas flowing. In Fig. 2, Patterns A to B, C to E, and F to

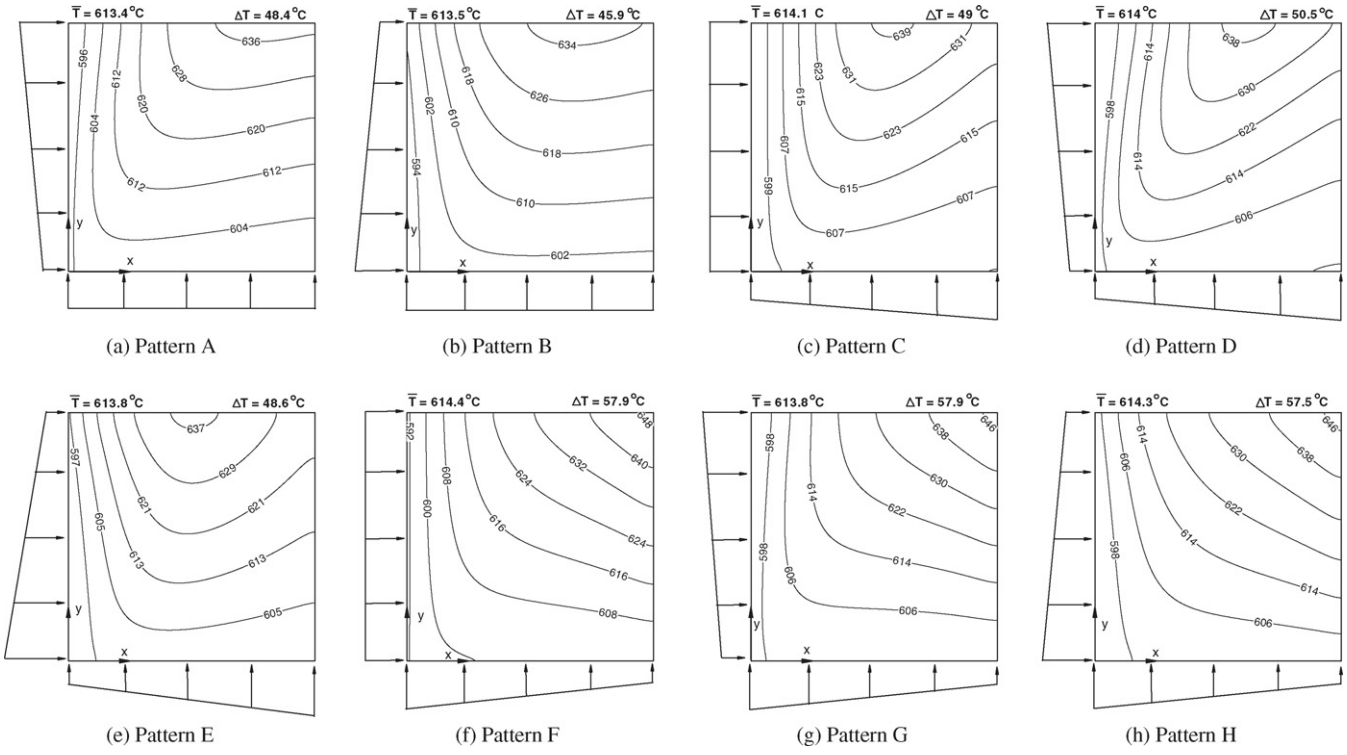

Fig. 6. Cell temperature distribution of eight non-uniform patterns with deviation of 0.5.

H have the same inlet flow profile of the cathode gas in each group. In Fig. 6(a) and (b), the cell temperature distributions of Patterns A and B are similar, and the main trend of cell temperature increases from under 600 °C in the inlet of cathode gas to 636–638 °C in the outlet of the cathode gas along the *y* direction, which is close to that in Fig. 3 with uniform inlet flow of the anode and the cathode gases. The cell temperature distribution of Patterns C, D, and E are similar to each other, and Fig. 6(c–e) show that the isotherm range is from under 600 °C to 638–640 °C, and the highest temperature moves from the corner of the outlet of both cathode gas and anode gas to the middle of the cathode gas outlet. Examining the inlet flow profile of Patterns C to E indicates that the flow rate of cathode gas progressively increases in the *x* direction. Since the part that is close to the outlet of the anode gas has more cathode gas to cool the cell, the highest temperature in the corner moves to the left, as revealed by comparing Fig. 6(a) and (b), which have uniform cathode inlet flow. In Fig. 6(f–h), Pattern F, G, and H also have analogous temperature distribution of the cell, and these figures show that the temperature distribution of the cell is from under 600 °C to 648–649 °C, and the highest temperature occurs in the corner of the outlet of the cathode gas and the anode gas. Notably, the variation of cell temperature in Patterns F to H is about 58 °C, and it is wider than that in Patterns A to E, so this is the worst temperature distribution. Patterns F to H have the same inlet flow profile of the cathode gas, which is progressively decreasing in the *x* direction. This non-uniform inlet flow causes less cathode gas to flow through the part with higher temperature on the cell, where is near the outlet of the anode gas. Therefore, the highest temperature in Fig. 6(f–h) rises more than those in Fig. 6(a–e). This study selects the cell temperature field of Pattern B and F, which has the least and most temperature variation, to subtract the cell temperature field in uniform pattern, and then show the results in Fig. 7. In this figure, the temperature difference of Pattern B related to uniform pattern is between −3 and 5 °C, as well as the largest temperature difference of Pattern F related to uniform pattern occurs at the corner of gas outlet and it is over 12 °C.

Fig. 8 plots the systematic cell current density distribution of eight inlet flow patterns with a deviation of 0.5. Meanwhile, $\bar{i}$ and Δi represent the average and the variation of current density, respectively. In this figure, the current density distribution of Pattern A is similar to those of Patterns D and G, and that of the current density distribution of Pattern B is analogous with those of Patterns E and H. Similarly, the current density distribution of Pattern C is similar to that of Pattern F. The inlet flow profile of each pattern in Fig. 2 indicates that Patterns A, D, and G, Patterns B, E, and H, and Patterns C and F represent three groups whose members have same profile of anode gas inlet flow in each group. Therefore, the inlet flow pattern of the anode gas dominates the current density distribution. As mentioned in the second paragraph of this section, the concentration of hydrogen and the total resistance of the cell influence the current density. An anode gas flows faster with a less varying hydrogen concentration, and with a more uniform current density distribution as the uniformity of the Nernst voltage increases. On the contrary, an anode gas flows more slowly and with a greater change in the hydrogen concentration because of the consumption of hydrogen in the chemical reaction, with a greater change of current density in the direction of flow of the anode gas. In

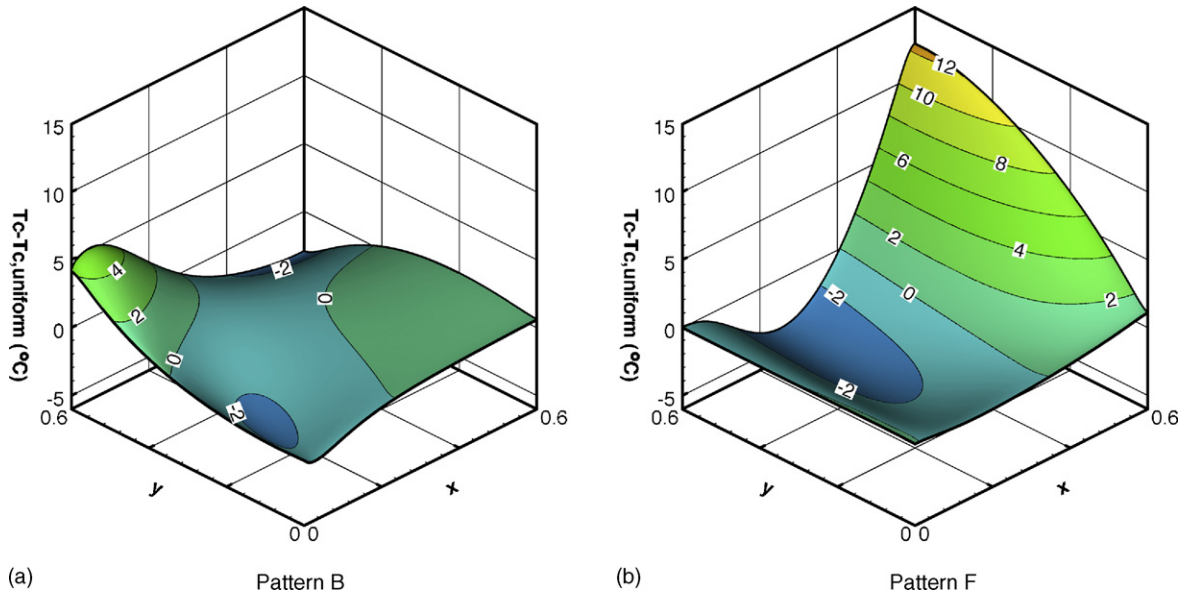

Fig. 7. Temperature difference related to uniform pattern on the cell plane.

Fig. 8(c–f), the current density distributions are similar to that in Fig. 4 because the inlet flows of anode gas has the same uniform profile. In Fig. 8(a), (d), and (g), it is clear that the current density distribution at the top half of the cell is clearly more uniform than that in the bottom half of the cell, because the inlet flow of anode gas in Patterns A, D, and G progressively increase in the y direction. Fig. 8(b), (e), and (h) show that the current density distribution is more uniform in the bottom half than in the top half of the cell, because Patterns B, E, and H have a progressively decreasing inlet flow rate of the anode gas in the y direction.

Fig. 9 shows that the current density difference of Pattern D and F related to the uniform pattern, because Pattern D and F has the most and least current density variation in Fig. 8. In Fig. 9(a), the current density difference of Pattern D is between −365 and 173 A m^{-2}, and the maximum difference occurs near the outlet of anode gas. The current density difference of Pattern F related to uniform pattern is between −30 and 53 A m^{-2}, so it seems flat in Fig. 9(b).

This study calculates all patterns in Fig. 2 with three deviation of 0.25, 0.5 and 0.75. Table 3 presents the results and Fig. 10

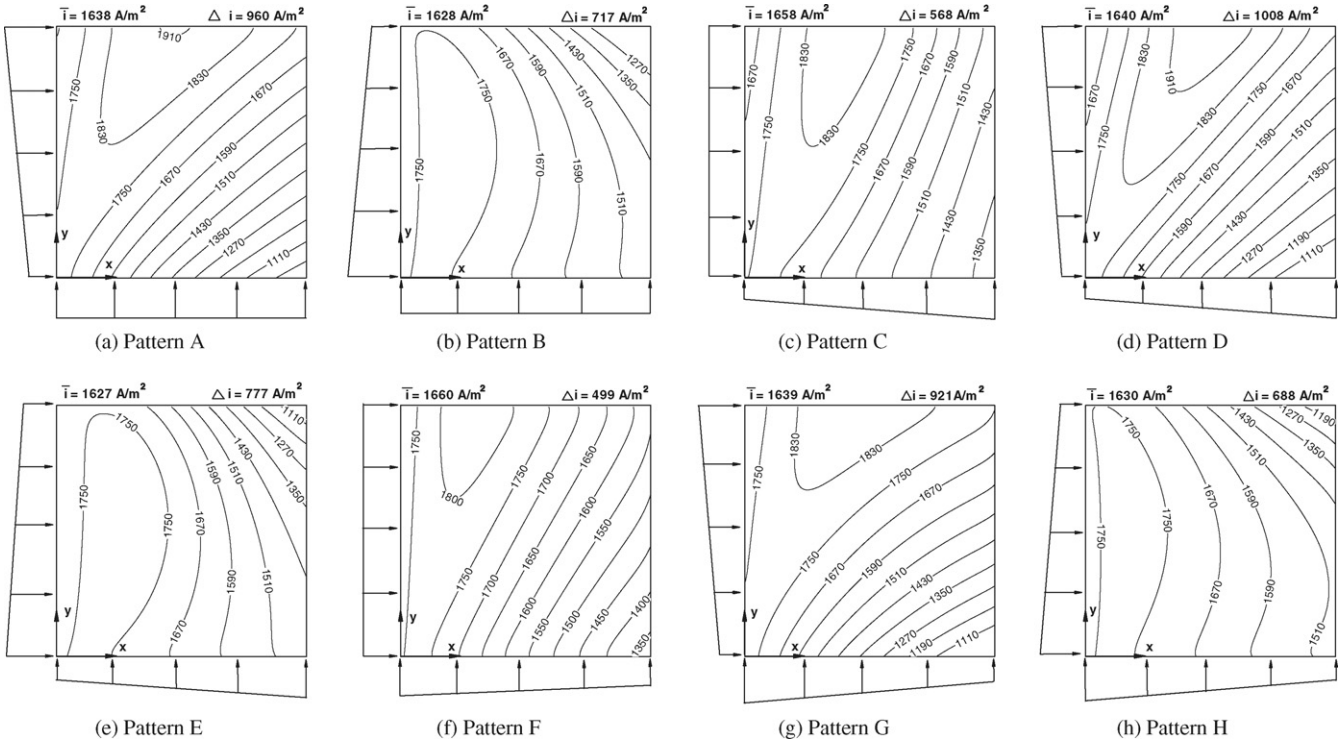

Fig. 8. Current density distribution of eight non-uniform patterns with deviation of 0.5.

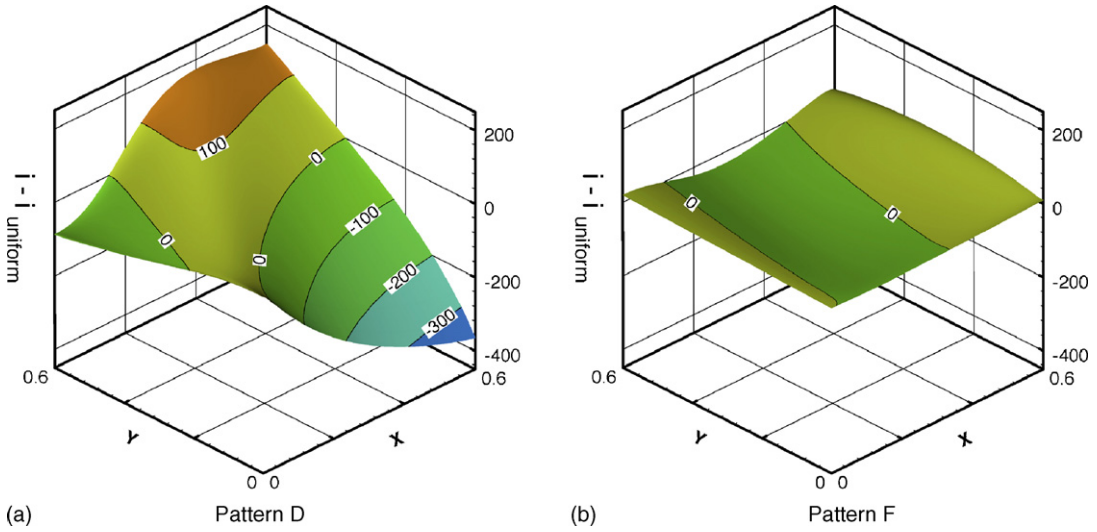

Fig. 9. Current density difference related to uniform pattern on the cell plane.

presents them as histograms. The vertical axis represents the relative variation of temperature or current density in non-uniform patterns to uniform pattern. Meanwhile, ΔT and Δi represent the difference between the maximum and minimum temperature and current density on the cell. In Fig. 10(a), the relative variation between average cell temperature and that in the uniform inlet flow is always $\pm 0.4\%$ for all deviations. Consequently, the non-uniform inlet flow affects slightly the average cell temperature and this effect can be ignored. In Fig. 10(b), the absolute relative variation between the average current density and that in uniform inlet flow is always lower than 5% for all deviations. The variation between average current densities in Pattern C and F are clearly close to zero, indicating that if the inlet of the anode gas is kept uniform, then a drop in the average current density can be avoided, even when the inlet of the cathode gas is non-uniform. Additionally, the relative variations of average current density in Patterns B, E and H are much worse than in the other patterns, and are close to -5% at a deviation of 0.75. Examining the patterns in Fig. 2 shows that all of them have progressively decreasing inlet flow in anode gas. Based on Eqs. (11) and (14), increasing the cell temperature increases the Nernst voltage and reduces the total cell resistance. Therefore, the current density increases with the cell temperature as the Nernst voltage gets increases and total cell resistance in Eq. (13) declines. According to the results in Figs. 6 and 8, the temperature and the current density in the top part of the cell plane are higher than those in the bottom part. The higher current density causes more hydrogen to be consumed in this area. Therefore, the consumption of hydrogen in this area is more than that in other area due to the higher current density. In Patterns B, E, and H, since the mole flow rate in the top part is less than that in the bottom part due to the progressively decreasing inlet profile of anode gas, the average current density will drop due to the lack of hydrogen. Therefore, the progressively decreasing inlet flow profile in anode gas is the worst for average current density.

Fig. 10(c) and (d) represent the relative variation of cell temperature and current density distribution related to those in uniform inlet flow. The distribution of temperature is worst in Pattern F with a deviation of 0.75, for which the relative variation is 37%. The distribution of current density is worst in Pattern D with deviation of 0.75, for which the relative variation is 179%. Furthermore, authors find that some relative variations are negative in Fig. 10(c) and (d), indicating that the variation of temperature or current density in the non-uniform inlet flow is less than that in uniform flow. In Fig. 10(c), Pattern B exhibits a better distribution of temperature because the temperature difference decreases as the deviation of non-uniform profile increases. Moreover, Pattern F has a more intensive current

Table 3
Relative variation of cell temperature and current density at different non-uniform inlet flow patterns related to at uniform inlet flow pattern

	$\frac{\bar{T}_c-\bar{T}_{c,uniform}}{\bar{T}_{c,uniform}}(\%)$			$\frac{\bar{i}_c-\bar{i}_{c,uniform}}{\bar{i}_{c,uniform}}(\%)$			$\frac{\Delta T_c-\Delta T_{c,uniform}}{\Delta T_{c,uniform}}(\%)$			$\frac{\Delta i_c-\Delta i_{c,uniform}}{\Delta i_{c,uniform}}(\%)$		
	$d=0.25$	$d=0.5$	$d=0.75$	$d=0.25$	$d=0.5$	$d=0.75$	$d=0.25$	$d=0.5$	$d=0.75$	$d=0.25$	$d=0.5$	$d=0.75$
A	−0.0160	−0.0676	−0.1907	−0.1833	−1.1626	−3.5033	2.4545	3.2414	2.0600	33.0081	81.0958	164.6495
B	−0.0121	−0.0499	−0.0814	−0.4891	−1.8122	−4.5346	−0.0149	−2.0771	−7.2740	−15.3020	35.2631	131.6049
C	0.0143	0.0582	0.1193	−0.0026	−0.0055	−0.1369	0.8594	4.5487	10.3150	3.6401	7.1689	12.0035
D	0.0063	0.0328	0.0607	−0.1659	−1.0670	−3.3795	3.3161	7.7346	9.5686	36.9351	90.1642	179.2814
E	−0.0026	0.0005	0.0095	−0.5184	−1.8799	−4.7295	1.1046	3.5997	5.9902	−8.5275	46.5420	141.3524
F	0.0330	0.0992	0.2094	0.0403	0.0949	−0.0313	9.4151	23.5280	37.2358	−2.8645	−5.8102	−9.9523
G	0.0089	0.0040	−0.0438	−0.1568	−1.1202	−3.5865	11.5262	23.4491	28.7527	29.5586	73.8560	154.2792
H	0.0350	0.0888	0.1626	−0.4400	−1.6696	−4.4963	9.2487	22.6260	33.8558	−21.0292	29.8983	147.1528

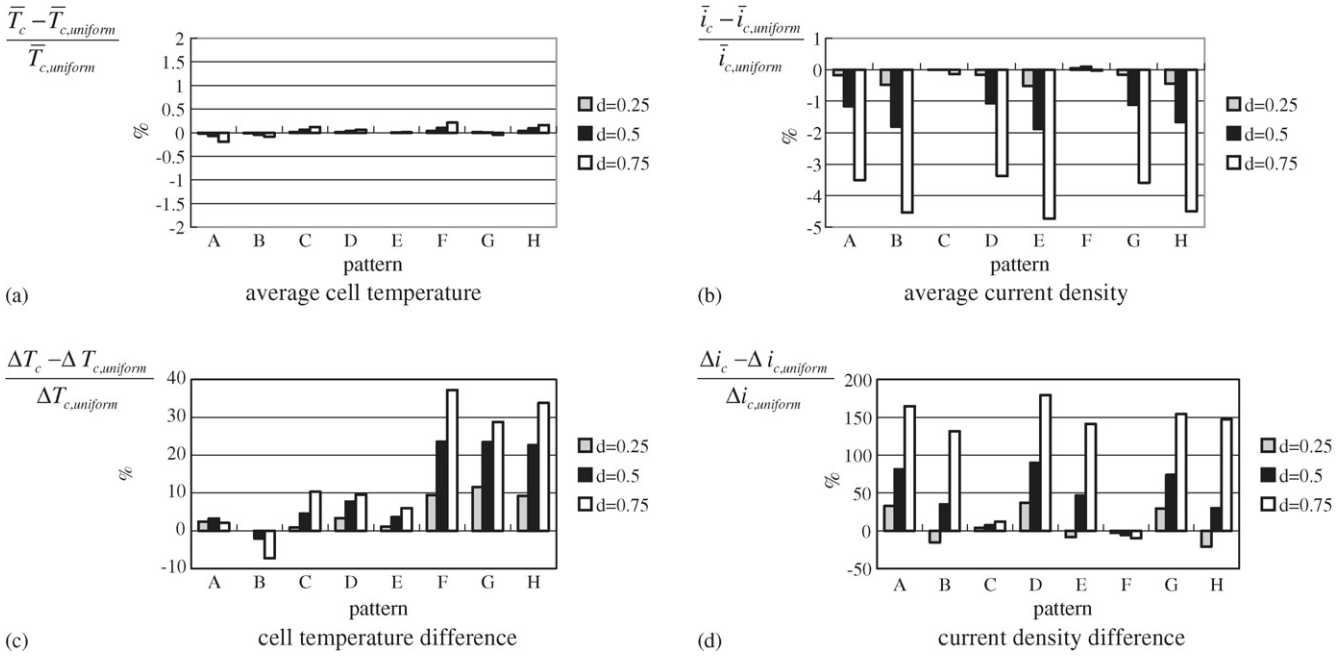

Fig. 10. Relative variation of cell temperature and current density at different non-uniform inlet flow patterns related to at uniform inlet flow pattern.

density distribution than that in uniform in Fig. 10(d), because the values of relative variations are −3%, −6%, and −10% with deviations of 0.25, 0.5, and 0.75, respectively. Although Pattern B has a better temperature distribution than the uniform pattern and Pattern F has a better current density distribution than the uniform pattern, the current density distribution in Pattern B is worsen because of the non-uniform inlet flow of the anode gas, as well as the temperature distribution in Pattern F is worsen because of the non-uniform inlet flow of the cathode gas. In Fig. 10(c) and (d), note that both Patterns A and B have better temperature distribution than the other non-uniform patterns, and both Patterns C and F have a better current density distribution than the other non-uniform patterns. Examining the inlet flow profile in Fig. 2 indicates that Pattern A and B have uniform inlet flow of cathode gas, and Pattern C and F have uniform inlet flow of anode gas. Therefore, the uniform inlet flow in both the anode side and the cathode side is the best profile from the perspective cell temperature and current density distribution. In industrial applications, the position of the inlet manifold affects primarily the inlet flow distribution and the uniform inlet profile is difficult to obtain. Therefore, the uniform inlet flow is the goal of the design of an MCFC with a cross-flow configuration, and designers must avoid putting the inlet manifolds of the anode gas and the cathode gas too close to the side of another gas inlet, which would produce non-uniform inlet flow with a progressively decreasing profile. Such poor positions of manifolds would further reduce average current density, as shown in Patterns B and E in Fig. 10(b), and widen the cell's temperature distribution, as shown in Patterns F to H of in Fig. 10(c).

5. Conclusions

Non-uniform inlet flow rates of anode gas and cathode gas are practical because of the position of the manifold and the distributor geometry in a molten carbonate fuel cell. This study considered uniform, progressively increasing, and progressively decreasing profiles in the anode gas and the cathode gas, as well as combinations of these profiles in the form of eight patterns of non-uniform inlet flow. Mass conservation, energy conservation and electrochemistry equations were considered, and the variation in the z direction ignored. Through the accuracy comparison in cell temperature and current density distribution, this study established the reliable numerical method by Fortran program. This study plots the temperature distribution and current density distribution on the cell plane in different patterns and draws the following conclusions. The cathode gas dominates the temperature distribution of the cell because of its flow rate exceeds that of the anode gas. The cell temperature is highest in the corner of the outlet of the anode gas and the cathode gas in a uniform inlet flow pattern. The progressively increasing profile of the cathode gas moves the hot spot in the corner to the middle of cathode gas outlet. The progressively decreasing profile of the cathode gas increases the temperature of the hot spot in the corner, and degrades the temperature distribution. Therefore, the position of the inlet manifold of the cathode gas must not be near the corner of the cathode gas inlet and the anode gas inlet, because it would then cause the progressively decreasing profile of inlet flow, and widen the cell temperature distribution. The anode gas dominates the current density of the cell because of the hydrogen concentration. The progressively increasing profile of the anode gas leads to the largest variation of the current density, and the progressively decreasing profile of the anode gas leads to the lowest average current density. This result implies that the uniformity of the anode gas in the inlet is important to the design of distributors. Moreover, the non-uniform inlet flow only slightly affects the average temperature and the current density of cell, but it influences more strongly the range and contour outlines of cell

temperature and current density. For example, the temperature variation on the cell plane in Pattern G and the current density variation on the cell plane in Pattern D are 12% and 37% higher than those of the uniform pattern, respectively, when the deviation of the non-uniform profile is 0.25. Therefore, the effect of the inlet flow maldistribution on the temperature and current density distribution on the cell plane is apparent, and cannot be neglected as the deviation of the profile increases.

Acknowledgements

The authors would like to express appreciation to Professor Barbara Bosio for her valuable comments. The authors gratefully acknowledge support for this study from the National Science Council of the Republic of China, Taiwan, project No. NSC 93-2212-E-009-001.

References

[1] N. Kobayashi, H. Fujimura, K. Ohtsuka, JSME Int. J., Ser. II 32 (1989) 420–427.
[2] F. Yoshiba, N. Ono, Y. Izaki, T. Watanabe, T. Abe, J. Power Sources 71 (1998) 328–336.
[3] F. Yoshiba, T. Abe, T. Watanabe, J. Power Sources 87 (2000) 21–27.
[4] J.H. Koh, B.S. Kang, H.C. Lim, AIChE J. 47 (2001) 1941–1956.
[5] J.H. Koh, H.K. Seo, Y.S. Yoo, H.C. Lim, Chem. Eng. J. 87 (2002) 367–379.
[6] W. He, Q. Chen, J. Power Sources 55 (1995) 25–32.
[7] W. He, Q. Chen, J. Power Sources 73 (1998) 182–192.
[8] B. Bosio, P. Costamagna, F. Parodi, Chem. Eng. Sci. 54 (1999) 2907–2916.
[9] E. Arato, B. Bosio, P. Costa, F. Parodi, J. Power Sources 102 (2001) 74–81.
[10] M. Mangold, M. Sheng, Fuel Cells 4 (2004) 68–77.
[11] Y.R. Lee, M.J. Yoo, G.Y. Chung, H.C. Lim, T.H. Lim, S.W. Nam, S.A. Hong, Korean J. Chem. Eng. 22 (2005) 219–227.
[12] B. Bosio, P. Costamagna, F. parody, B. Pasalacqua, J. Power Sources 74 (1998) 175–187.
[13] H. Hirata, M. Hori, J. Power Sources 63 (1996) 115–120.
[14] P. Yuan, H.S. Kou, Numer. Heat Transfer, Part A 43 (2003) 619–638.
[15] S.V. Patankar, Numerical Heat Transfer and Fluid Flow, Hemisphere, New York, 1980, p. 37.
[16] L.J.M.J. Blomen, M.N. Magerwa, Fuel Cell Systems, Plenum Press, New York, 1993, pp. 73–75.